A numerical simulation of steady state metal cutting

Pierre Joyot, Roger Rakotomalala, Olivier Pantalé, Maurice Touratier, N Hakem

A numerical simulation of steady state metal cutting

P Joyot[1], **R Rakotomalala**[1], **O Pantalé**[1], **M Touratier**[2] and **N Hakem**[3]
[1]Laboratoire Génie de Production, CMAO-ENIT, Tarbes, France
[2]LM2S-URA CNRS 1776 UPMC-ENSAM-ENS Cachan, Paris, France
[3]Renault, Rueil Malmaison, France

Abstract: An arbitrary Lagrangian–Eulerian (ALE) approach is used to model the orthogonal metal cutting in a steady state situation. The thermomechanical model includes the effects of elasticity, plasticity, strain rate, large strains and friction with heat generated between the tool and the chip. The ALE formulation can combine the advantages of both the Eulerian and Lagrangian approaches in a single description. Particularly, problems linked to the free surface in a Eulerian description and those linked to severe mesh distortions in a Lagrangian one can be solved by this formulation. The ALE governing equations are briefly reviewed in this paper; finite element and finite volume methods are used for the discretization of the conservation equations and an explicit time integration is adopted. Only the steady state solution is required; the ALE formulation is exploited to update the free and the contact surfaces. The model predicts the thermomechanical quantities, the chip geometry and the cutting forces from the cutting data and the material and friction parameters.

Cutting experiments were performed with 42CD4 steel and comparisons of experimental tool forces and chip geometry with the numerical results are presented.

Keywords: metal cutting, arbitrary Lagrangian–Eulerian, finite element, finite volume, explicit integration, free surface

NOTATION

a_c	depth of cut
$A_{i(i=e,w,n,s)}$	surface of one side of the finite volume mesh
c	specific heat
$\boldsymbol{C}$	convective velocity
C_f	frictional coefficient
e	specific internal energy
$\boldsymbol{f}$	specific volume force
$\boldsymbol{F}_f$	frictional force
$\boldsymbol{K}$	constitutive tensor
n_i	normal vector on the surface A_i
q	heat flux density
$\boldsymbol{q}$	heat flux vector
T^*	non-dimensional temperature (K) $=(T-T_{ref})/(T_{melt}-T_{ref})$ where $T_{melt}=1793$ K, $T_{ref}=300$ K
$\boldsymbol{V}$	material velocity
V_c	cutting speed
$\boldsymbol{W}$	grid velocity
x_i	Eulerian coordinates
$\dot{\varepsilon}$	strain rate tensor
ξ_i	arbitrary coordinates
ρ	material density
σ	Cauchy stress tensor
σ_0	flow stress

1 INTRODUCTION

Experimental observations of the flow pattern in metal-cutting processes show the complexities of the phenomena associated with this process. The work material is subjected to high strains, high strain rates and elevated temperatures. The interaction between the cutting tool and the workpiece is also highly complex; the friction in the 'tool–chip' interface can create excessive temperatures and stresses. These complexities are the source of different sorts of non-linear aspects in governing equations. Therefore, most analytical and numerical investigations of metal-cutting processes are relative to orthogonal cutting (the shear plane problem). A review of analytical works is given by Strenkowski and Carroll [**1**] and by Oxley [**2**]. Generally, these analytical models are based on the slip line theory or the energy method, and predict tool forces, chip geometry and mean temperature.

In the past two decades, finite element methods have been progressively applied to simulate the metal-cutting process. The numerical simulations are more accurate and supply more detailed information, such as stresses, plastic strains, strain rates, temperatures and residual stress distributions. The existing numerical models for metal cutting are usually based on updated Lagrangian or Eulerian formulations. Strenkowski and Carroll give an updated Lagrangian method in reference [**1**], in which both the workpiece and the tool are discretized with a finite element mesh. The model can simulate the transient chip formation and the steady state situation. This fact gives a certain advantage to the Lagrangian approach; in addition, the free surfaces are obtained in a direct way. However, a significant limitation of this formulation is encountered when the solid deformations become large, as in the metal-cutting case; the severe distortions of the finite element mesh affect the accuracy of the solution. The authors propose a chip separation criterion at the tool tip; to allow for separation of the chip from the workpiece, the model employs a material parting criterion based on the effective plastic strain in the tool tip region of the work chip. Results from the model indicate that varying the separation criteria has little effect on the resulting chip geometry and tool forces. However, variations of the criteria over the range 0.25–1.0 significantly affect the stress field and the residual stresses in the workpiece. An updated Lagrangian method is also used by Childs and Maekawa [**3**] to predict the chip flow and stresses, tool temperatures and wear in metal turning; an initial guess is required of the shape of the chip. A similar approach is used by Komvopoulos and Erpenbeck [**4**] to analyse the effects of certain singularities like a built-up edge and crater on the tool. More recently, Shi and Yang [**5**] have used the updated Lagrangian formulation for a thermomechanical cutting model. An element separation criterion, which is based on the distance between the tool tip and the nodal point ahead of the tool, is adopted. A mesh rezoning technique is applied to cope with the severe mesh distortions. Different physical variables, such as strains, stresses, temperatures and residual stresses are analysed. The numerical predictions of the distributions of residual stresses show good agreement of the trend, as compared with X-ray measurements.

A Lagrangian approach is also used by Shekon and Chenot [**6**] and Marusich and Ortiz [**7**] for the orthogonal metal-cutting modelling. Continuous remeshing and adaptative meshing are the principal tools which the authors employ for side-stepping the difficulties associated with the deformation-induced element distortion.

Another approach for developing finite element modelling of cutting processes is to use a Eulerian formulation. Generally, this approach is suitable to simulate a steady state process, particularly when the flow geometry is known. A formulation of this type is presented by Zienkiewicz and co-workers [**8**] for viscoplastic materials; extrusion and rolling problems are treated to illustrate the strategy. In the context of metal cutting, Strenkowski and Moon [**9**] have used a similar approach to obtain a steady state solution. An iterative scheme is introduced to obtain the steady free surfaces; a requirement of the steady state solution is that the final velocity is tangential to the free surface. Compared to an updated Lagrangian approach, the problems associated with mesh distortions and separation criterion of the chip from the workpiece are avoided in a Eulerian formulation.

In the past few years, the arbitrary Lagrangian–Eulerian (ALE) formulation for simulating fluid/structure interactions and forming processes has been used by several authors [**10**–**12**] in order to overcome problems met when using purely Eulerian or purely Lagrangian formulations. In this paper, the ALE formulation is used to model orthogonal metal cutting with a continuous chip. This approach can combine the advantages of both the classical approaches in a single description and can be considered as a method with automatic and continuous rezoning. The model is ALE until the steady state conditions are reached. This permits free and contact surfaces especially to be updated. Then, once these conditions are obtained, this model is equivalent to a Eulerian one. In a previous work [**13**], this method was used to predict the thermomechanical variables only in the workpiece. In this study, the heat generation due to the friction in the tool–chip interface is taken into account. The thermomechanical model takes into account an elastoplastic constitutive law for the work material and a Coulomb friction law with heat generation in the tool–chip interface. Hence, the temperatures, the stress and strain fields in the workpiece, the tool forces and the temperature in the tool can be predicted; no empirical data such as separation criterion, measured contact length or geometrical data chip are required to obtain these parameters. In addition, the model is used to analyse the influence of wear at the rake face of the tool. Cutting experiments were also performed with 42CD4 steel and comparisons of experimental cutting forces and chip geometry with numerical results were effected.

2 GOVERNING ALE EQUATIONS

In the ALE finite element or finite volume mesh, the grid points are not constrained to remain fixed in space (Eulerian) or to move with material points (Lagrangian). This provides more freedom in formulating the mathematical model.

The material motion is defined by the classical relation $\boldsymbol{x} = \boldsymbol{\phi}(\boldsymbol{X}, t)$ [or $x_i = \phi_i(X_j, t)$], where $\boldsymbol{x}$ denotes the position occupied by the particle at time t and $\boldsymbol{X}$ its position at initial time. The material velocity $\boldsymbol{V}$ is obtained by

the material time derivative

$$\boldsymbol{V} = \dot{\boldsymbol{x}} = \left.\frac{\partial \boldsymbol{x}}{\partial t}\right|_{X}$$

The reference grid points are identified by a set of independent coordinates ξ_i; the grid motion is given by a relation $\boldsymbol{x} = \boldsymbol{\psi}(\xi, t)$ [or $x_i = \psi_i(\xi_j, t)$] which gives the grid velocity

$$\boldsymbol{W} = \mathring{\boldsymbol{x}} = \left.\frac{\partial \boldsymbol{x}}{\partial t}\right|_{\xi}$$

In a numerical treatment, the physical quantities are computed at geometrical points x_i occupied by the grid points at a time t. In the conservation laws, the material time derivative of a function $G(\boldsymbol{x}, t)$ is required. Hence, the following relation between the material time derivative ($\dot{G}$) and the referential time derivative ($\mathring{G}$) is applied to the classical Eulerian forms [**1**]:

$$\dot{G} = \mathring{G} + \boldsymbol{C}\nabla G \tag{1}$$

where $\mathring{G}$ is the time derivative at a grid point that occupies the geometrical point x_i at time t and $\boldsymbol{C} = \boldsymbol{V} - \boldsymbol{W}$ is the so-called convective velocity.

In neglecting the radiation effects in the energy equation, the local ALE forms of the conservation laws are then given by

$$\mathring{\rho} + \boldsymbol{C}\nabla\rho + \rho \operatorname{div} \boldsymbol{V} = 0 \qquad \text{(mass)} \tag{2}$$

$$\rho\mathring{\boldsymbol{V}} + \rho\boldsymbol{C}\nabla\boldsymbol{V} = \boldsymbol{f} + \operatorname{div}\sigma \qquad \text{(momentum)} \tag{3}$$

$$\rho\mathring{e} + \rho\boldsymbol{C}\nabla e = \sigma : \dot{\varepsilon} - \operatorname{div}\boldsymbol{q} \qquad \text{(energy)} \tag{4}$$

where ρ is the mass density, $\boldsymbol{f}$ are the body forces, σ is the Cauchy stress tensor, e is the specific internal energy, $\dot{\varepsilon}$ is the strain rate tensor, $\boldsymbol{q}$ the heat flux vector and ∇ the Nabla operator.

A constitutive relationship for thermal elastoplastic materials is adopted in the model. The Cauchy stress tensor σ is decomposed into its deviatoric part $\mathbf{s}$ and the hydrostatic pressure p, where both are given by the incremental objective ALE forms as follows:

$$\mathring{\mathbf{s}} + \boldsymbol{C}\nabla\mathbf{s} = \mathbf{K} : \dot{\varepsilon} + \Omega\mathbf{s} - \mathbf{s}\Omega \tag{5}$$

$$\mathring{p} + \boldsymbol{C}\nabla p = p(\rho, e) \qquad \text{(equation of state)} \tag{6}$$

Equation (5) is obtained by using the Jaumann derivative, where Ω is the spin tensor and $\mathbf{K}$ the constitutive tensor. Total strain ε and strain rate $\dot{\varepsilon}$ are decomposed

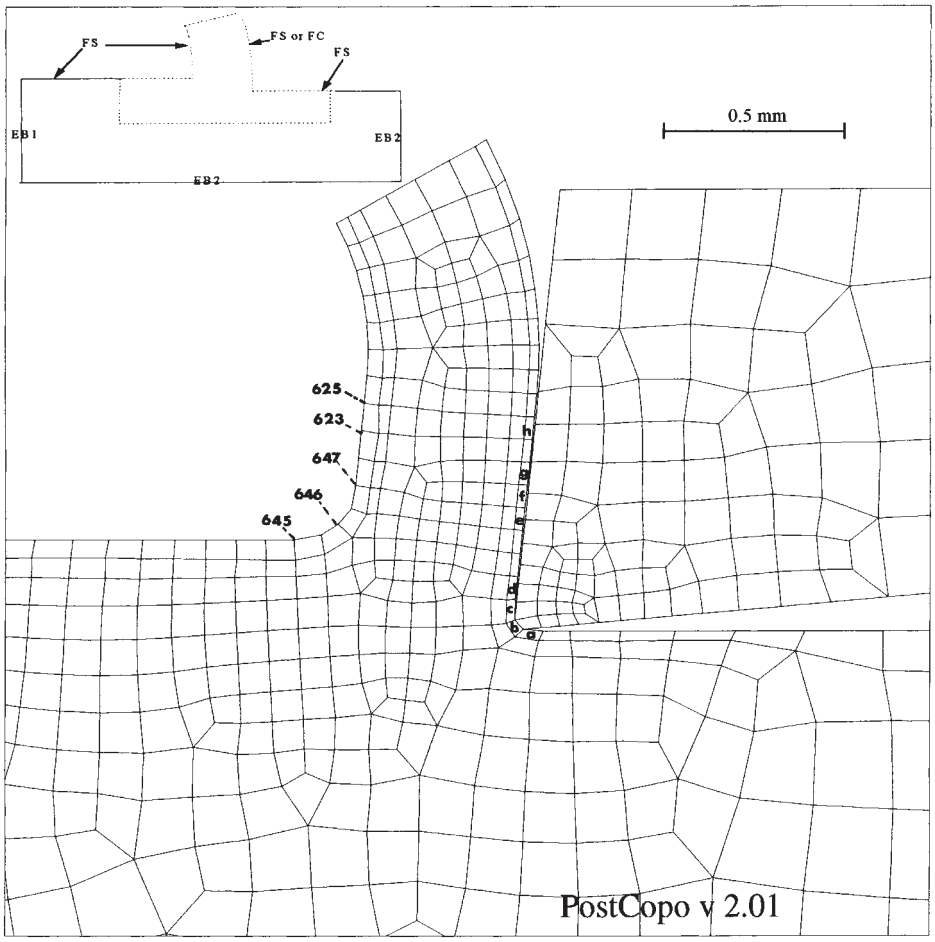

Fig. 1 Initial control volume with corresponding mesh and boundary conditions

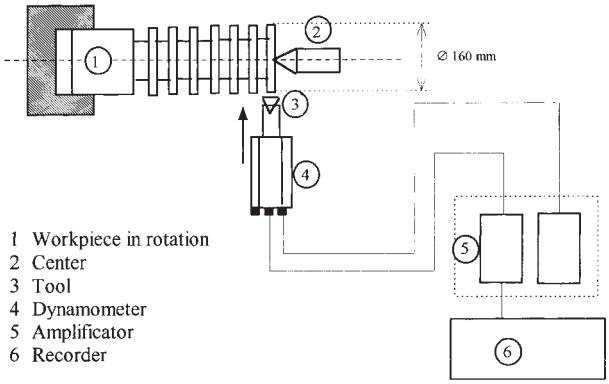

Fig. 2 Schematic diagram of the experimental set-up for force measurements: FS, free surfaces; CS, contact surface; EB1 and EB2, Eulerian boundary (prescribed velocity, material density and temperature on EB1); tool, Lagrangian structure with zero displacement; adiabatic conditions upon other boundaries except on CS; all other nodes, ALE

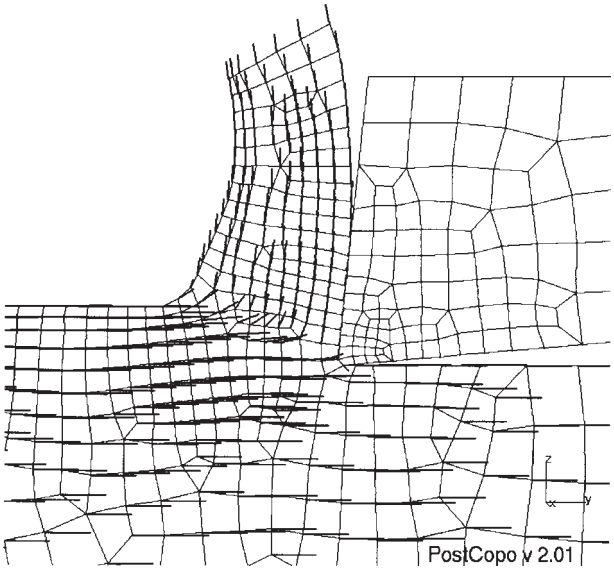

Fig. 3 Intermediate non-stabilized geometry of a chip with the corresponding velocity field

additively into an elastic part and a plastic part. The Johnson–Cook material law is adopted for the workpiece; assuming a von Mises yield criterion and an isotropic strain hardening rule, the flow rule is given by [**14**]

$$\sigma_0 = (A + B\bar{\varepsilon}^n)(1 + C \ln \dot{\bar{\varepsilon}}^*)(1 - T^{*m}) \tag{7}$$

where A, B, C, m, n are the material parameters and $\bar{\varepsilon}$, $\dot{\bar{\varepsilon}}^*$, T^* are respectively the equivalent strain, the adimensional equivalent strain rates and the non-dimensioned temperature. In the tool–chip interface, the Coulomb friction law is assumed and the stick/slip condition is given by [**13**] stick if $|T^{\mathrm{t}}| < C_{\mathrm{f}}|T^{\mathrm{n}}|$ and slip if $|T^{\mathrm{t}}| \geqslant C_{\mathrm{f}}|T^{\mathrm{n}}|$, where T^{n} and T^{t} are respectively the normal and the tangential components of the surface traction on the interface and C_{f} is the frictional coefficient. The heat generation in the slipping contact surface is given by $\mathrm{d}Q_{\mathrm{fric}} = |T^{\mathrm{t}}|\,|V^{\mathrm{t}}|\,\mathrm{d}t$, where V^{t} is the tangential slip velocity. In the model, it is assumed that the friction heat transmits in equal proportions between the workpiece and the tool.

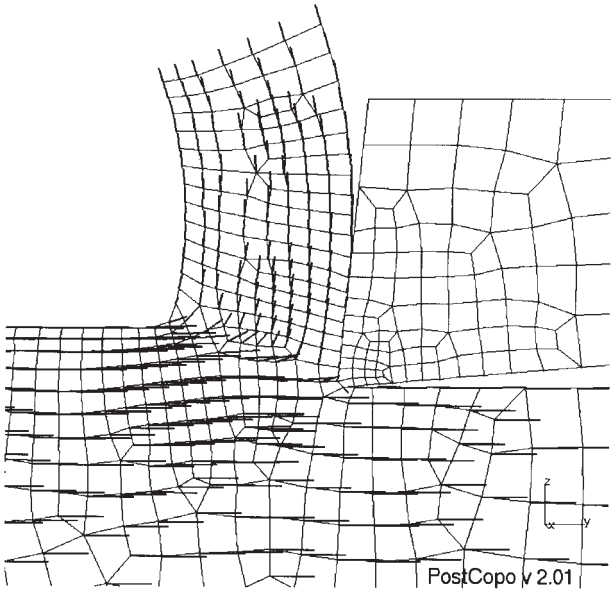

Fig. 4 Steady state geometry with the corresponding stabilized velocity field

The finite element method (FEM) is adopted for the discretization of the momentum equation (3). The weak form associated is obtained by multiplying this equation by a weighting function v_i^* over the spatial domain $\omega(t)$ with the boundary $\Gamma(t)$. Employing the divergence theorem to include the force vector $\boldsymbol{F}$ on the boundary Γ^F and using the Galerkin approach, the corresponding matrix equation is obtained:

$$\mathbf{M}^{\mathrm{v}}\mathring{\boldsymbol{V}} + \boldsymbol{F}^{\mathrm{trm}} + \boldsymbol{F}^{\mathrm{int}} + \boldsymbol{F}^{\mathrm{ext}} - \boldsymbol{F}^{\mathrm{hgr}} = \mathbf{0} \tag{8}$$

where $\mathbf{M}^{\mathrm{v}}$ is the mass matrix, $\boldsymbol{F}^{\mathrm{trm}}$ the momentum transport force vector, $\boldsymbol{F}^{\mathrm{int}}$ the internal stress vector and $\boldsymbol{F}^{\mathrm{ext}}$ the external force vector including the friction. Details of the finite element formulation and calculation of the different terms of equation (8) can be found in reference [**12**]. Four-node quadrilateral finite elements classically with a reduced integration rule are used in the present study, in order to improve the efficiency of the element in distorted situations and to reduce the computing cost; hence, corresponding zero energy modes must be controlled. The formulation proposed by Kosloff and Frazier [**15**] is adopted and $\boldsymbol{F}^{\mathrm{hgr}}$ represents the hourglass force control.

The mass and energy equations are discretized by a finite volume method (FVM) and the following

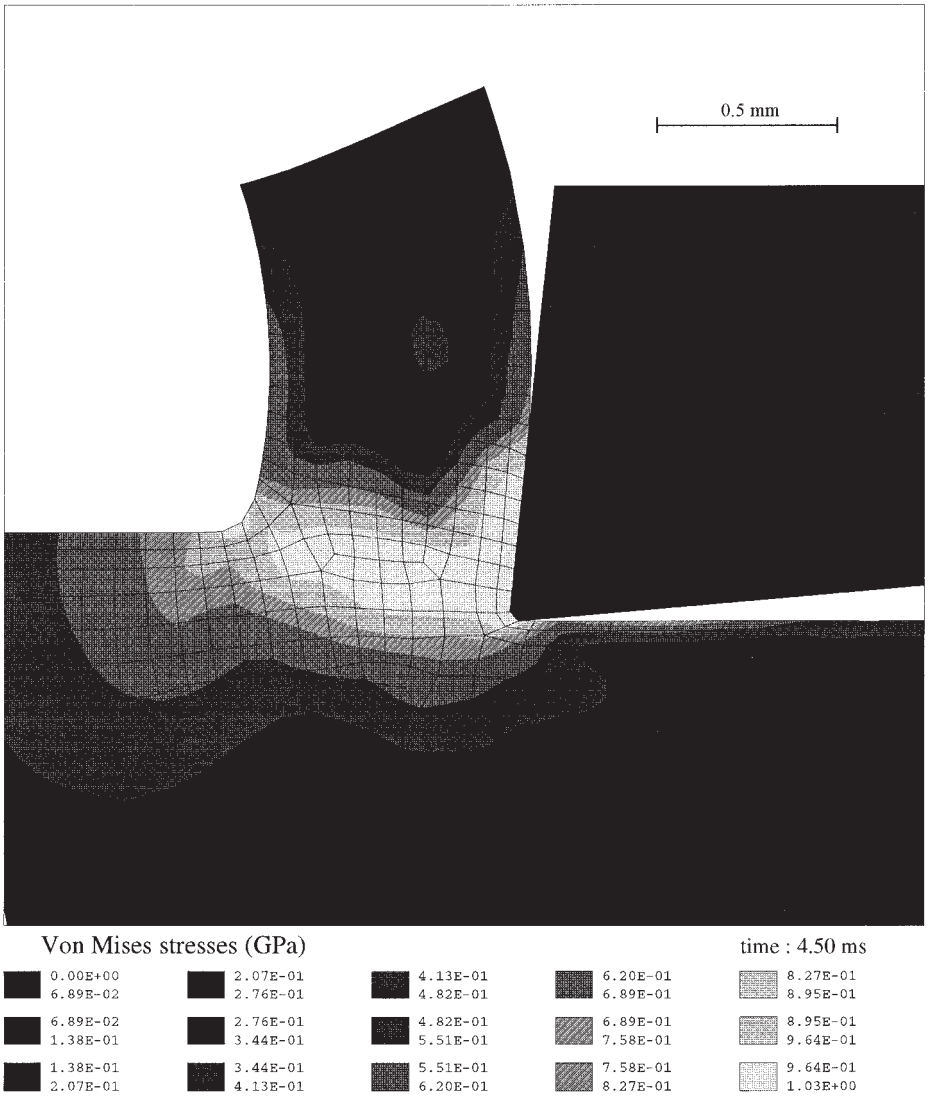

Fig. 5 Distribution of the von Mises stress (GPa) for the steady state solution

associated conservative forms are considered:

$$\left(\int_{\omega} \mathring{\rho}\, \mathrm{d}\omega\right) + \int_{\Gamma} \rho c_i n_i \, \mathrm{d}\Gamma = 0 \tag{9}$$

$$\left(\int_{\omega} \rho \mathring{e}\, \mathrm{d}\omega\right) + \int_{\Gamma} \rho e c_i n_i \, \mathrm{d}\Gamma = \int_{\Gamma} -q_i n_i \, \mathrm{d}\Gamma + \int_{\omega} \sigma_{ij} \dot{\varepsilon}_{ij} \, \mathrm{d}\omega \tag{10}$$

Using the notation of reference [**16**], the corresponding discrete relations are given by

$$0 = \mathring{\rho}_{\mathrm{p}} V + \sum_{i=\mathrm{e,w,n,s}} A_i \rho_i \boldsymbol{C} \cdot \boldsymbol{n}_i \tag{11}$$

$$(\rho \mathring{\boldsymbol{e}}_{\mathrm{p}}) V + \sum_{i=\mathrm{e,w,n,s}} A_i \rho_i e_i \boldsymbol{C} \cdot \boldsymbol{n}_i = V(\sigma : \dot{\varepsilon})_{\mathrm{p}} - \sum_{i=\mathrm{e,w,n,s}} A_i \boldsymbol{q} \cdot \boldsymbol{n}_i \tag{12}$$

From a geometric viewpoint, the finite volumes and finite elements are identical; the compatibility between the FEM and the FVM formulations is thereby ensured. In equations (11) and (12), V and A_i are respectively the volume and surfaces related to the finite volume cell; k_i is the value of the variable k at the point i (see Fig. 1). The convective terms, which characterize the ALE or the purely Eulerian formulations, imply difficulties linked to the stability of the solution: in equations (11) and (12), an upwind technique is used for the calculation of ρ_i and e_i. Concerning the energy equation, the classic Fourier law $\boldsymbol{q} = -k\nabla T$ is adopted where k is the conduction coefficient for an isotropic material and the specific internal energy e is linked to the temperature T by the classical relationship $\mathrm{d}e = c\, \mathrm{d}T$, where c is the specific heat.

For the time integration of equations (5), (6), (8), (11) and (12), an explicit central difference scheme of

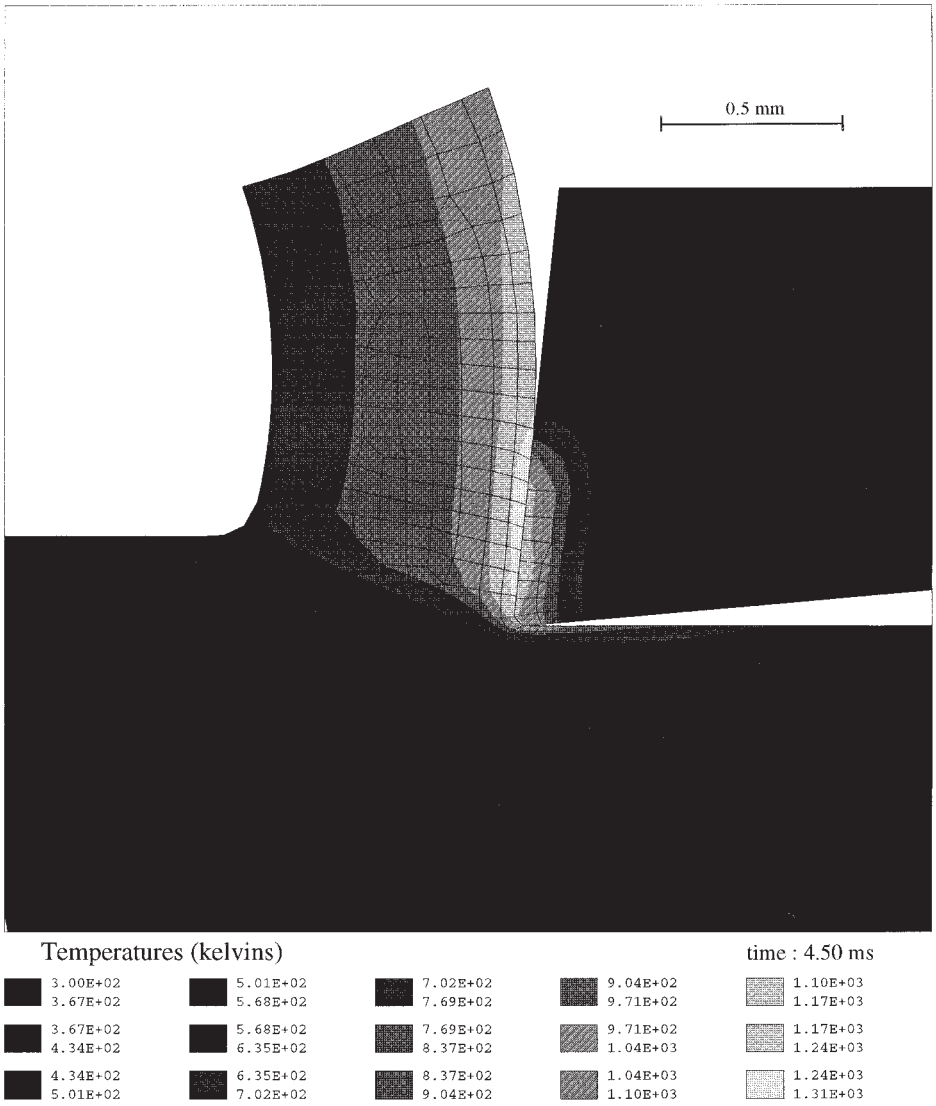

Fig. 6 Temperatures in the workpiece and the tool (K)

$(\Delta t)^3$ order of accuracy is used; the time step Δt is subjected with respect to the Courant stability condition [**16**]. For example, the calculation of the velocity is given by

$$\boldsymbol{V}^{t+\Delta t/2} = \boldsymbol{V}^{t-\Delta t/2} + \mathring{\boldsymbol{V}}^{t}\,\Delta t \tag{13}$$

The flow chart of the explicit computing procedure is as follows:

1. Initialization ($n = 0$); input initial conditions.
2. Time-stepping loop.
3. Integration of the grid velocity to obtain the mesh displacement and coordinates.
4. Calculate the incremental hydrostatic pressure, deviatoric stresses and internal force vector.
5. Compute acceleration.
6. Compute density, energy and temperature.
7. Integrate acceleration to obtain velocity.
8. Go to step 2 if the steady state solution is not obtained.

The computation is started with initial conditions on the boundaries where values are specified. The steady state solution is reached when the free surface condition is verified and if the different variables are stationary. In addition, the practical implementation of an ALE method requires an automatic mesh displacement prescription algorithm. The algorithm proposed by Giuliani [**17**], which is used in the model, is based on geometric criteria so as to minimize mesh distortions. The components of grid velocity at a typical ALE node I are computed at each step of the time integration procedure by the following relationship:

$$W_{I,i}^{t+\Delta t} = \frac{1}{N}\sum_{J} W_{J,i}^{t} + \frac{\alpha}{\Delta t}\sum_{J} L_{IJ}^{t} \sum_{J} \frac{u_J^t - u_I^t}{N^2 L_{IJ}^t} \tag{14}$$

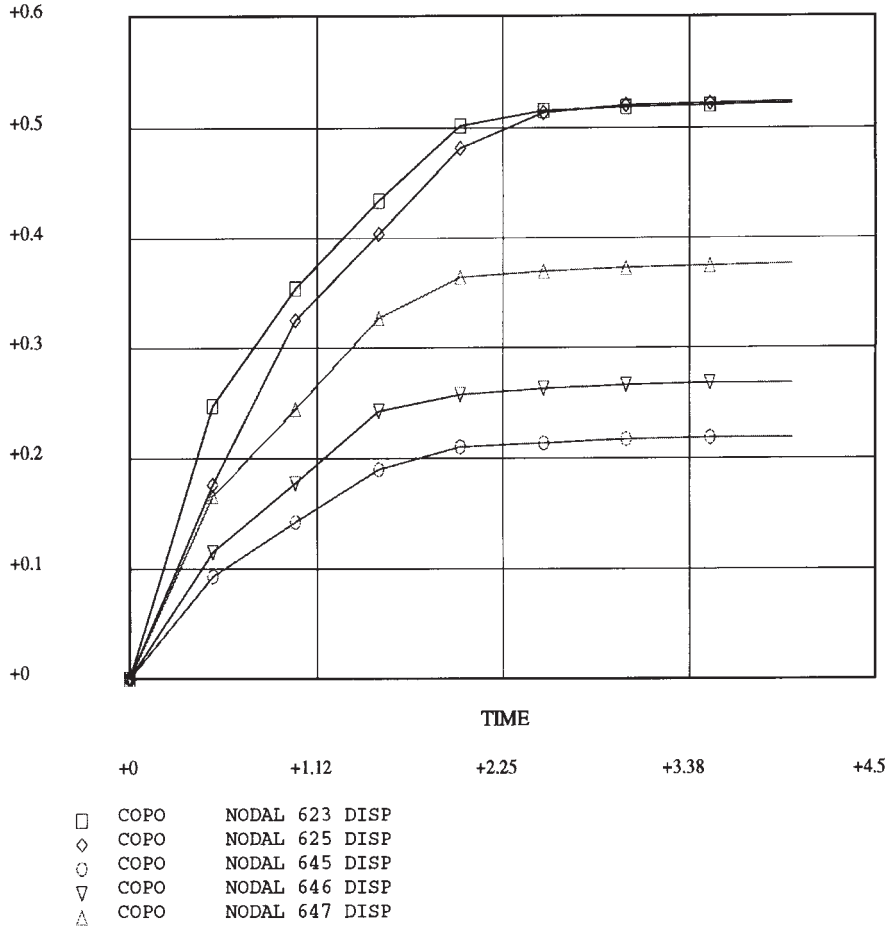

Fig. 7 Evolution of nodal displacements (μm) on the free surface versus computing time (ms) (see Fig. 1 for nodes localization)

Table 1 ALE and experimental values of cutting force (F_c), feed force (F_a) and chip thickness (CT). V_c = cutting speed; a_c = depth of cut

	$a_c = 0.25$ mm			$a_c = 0.5$ mm		
	$V_c = 1$ m/s	$V_c = 2$ m/s	$V_c = 4$ m/s	$V_c = 1$ m/s	$V_c = 2$ m/s	$V_c = 4$ m/s
F_c(exp) (± 20 N)	590 N	560 N	560 N	1000 N	990 N	930 N
F_c(ALE)	432 N	430 N	580 N	1050 N	1026 N	1020 N
F_a(exp) (± 20 N)	328 N	300 N	250 N	416 N	330 N	300 N
F_a(ALE)	226 N	210 N	165 N	360 N	358 N	352 N
CT(exp)	0.51 mm	0.51 mm	0.49 mm	0.9 mm	0.84 mm	0.88 mm
CT(ALE)	0.71 mm	0.7 mm	0.7 mm	1.11 mm	1.09 mm	1 mm

where N indicates the number of nodes connected to node I via sides and diagonals, L_{IJ} is the current distance between the node I and the connected node J and u represents the total node displacement.

3 THE ALE CUTTING MODEL

The model of orthogonal metal cutting presented in this work is relative to the steady state situation. The primary problem is due to the fact that the chip geometry and the contact length between the tool and the chip are not known in advance. The problem is treated from an initial arbitrary control volume, and the ALE formulation permits free and contact surfaces to be updated and a regular grid calculation to be kept. One of the requirements to obtain the solution is that the material velocity has a zero normal component at the free surfaces. In the ALE formulation, the nature of the nodes can be prescribed at the input. Therefore, a Eulerian node has a zero grid velocity ($\boldsymbol{W} = 0$), while a Lagrangian node moves with

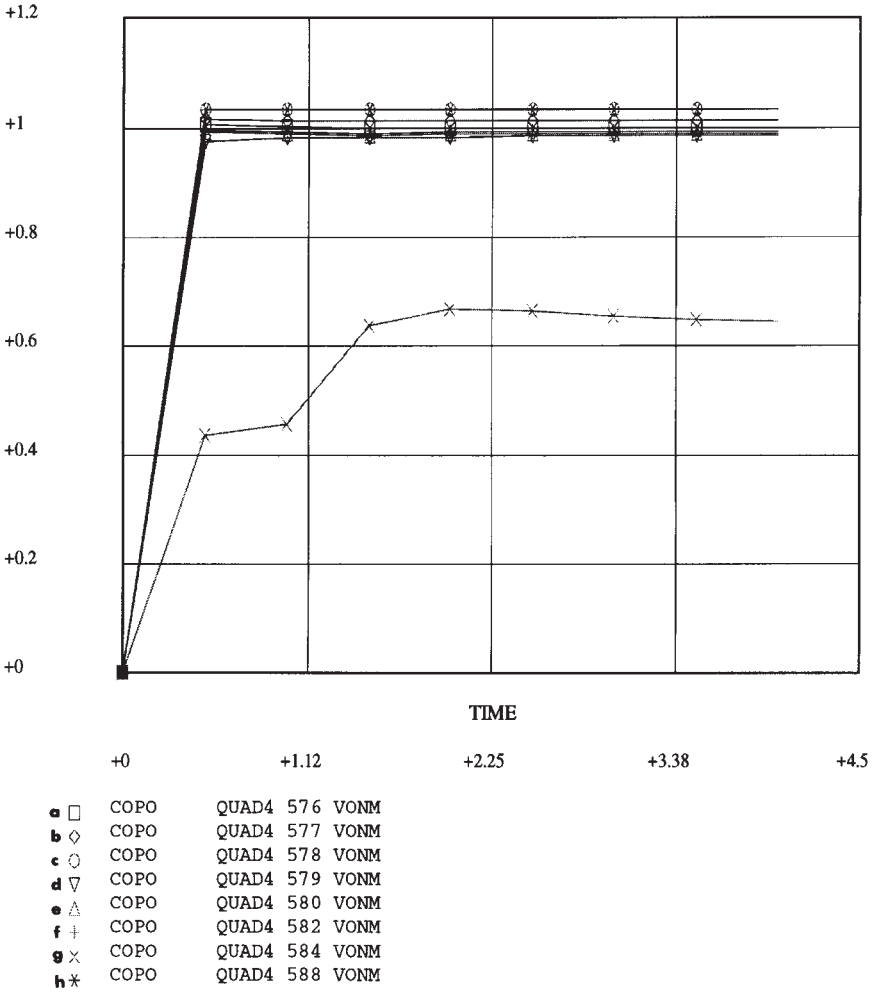

Fig. 8 Evolution of equivalent plastic strain in the vicinity of the contact surface versus computing time (ms) [see Fig. 1 for elements (QUAD4) localization]

the material point ($\boldsymbol{W} = \boldsymbol{V}$). Then, in the steady state simulation, the following specifications are attributed to the nodes upon the free and contact surfaces: Eulerian in the tangential direction and Lagrangian in the normal direction. The objective is to keep a regular node repartition along the free surface; then the normal displacement permits the free surface to be updated. A part of the initial arbitrary control volume is illustrated in Fig. 1. This figure also contains the prescribed nature of the nodes and the boundary conditions. Initially, only the two nodes at the tip tool are in contact with the tool because the contact length is unknown. The material parameters for 42CD4 steel, given by reference [**18**], are the following:

$E = 210$ GPa, $\quad v = 0.3$

$A = 595$ MPa, $\quad B = 580$ MPa, $\quad C = 0.023$

$m = 13$, $\quad n = 0.1$

Specific heat $c = 358$ J/kg K

Conductivity $k = 38$ W/m^2 K

The friction coefficient C_f was obtained on an experimental basis by applying a normal force to the tool in contact with the moving workpiece and by measuring the corresponding tangential forces. The value of $C_f = 0.32$ is adopted for the numerical simulations.

4 EXPERIMENTAL PROCEDURES

A series of experimental cutting was performed to validate the ALE cutting model. The workpiece is a 42CD4 steel and machining tests were conducted on a lathe under dry conditions. The work material composition is: Fe(97.078%), C(0.443%), Si(0.282%), Mn(0.731%), P(2.4%), S(2×10^{-3}%), Cr(1.022%), Mo(0.247%). The experimental set-up used to conduct validation is presented in Fig. 2. A carbide tool with a positive rake angle of 6°, a flank angle of 6° and a bevelled edge of 0.07 mm was used. The specific heat and the thermal conductivity of the tool are equal to 100 J/kg K and 25 W/m^2 K

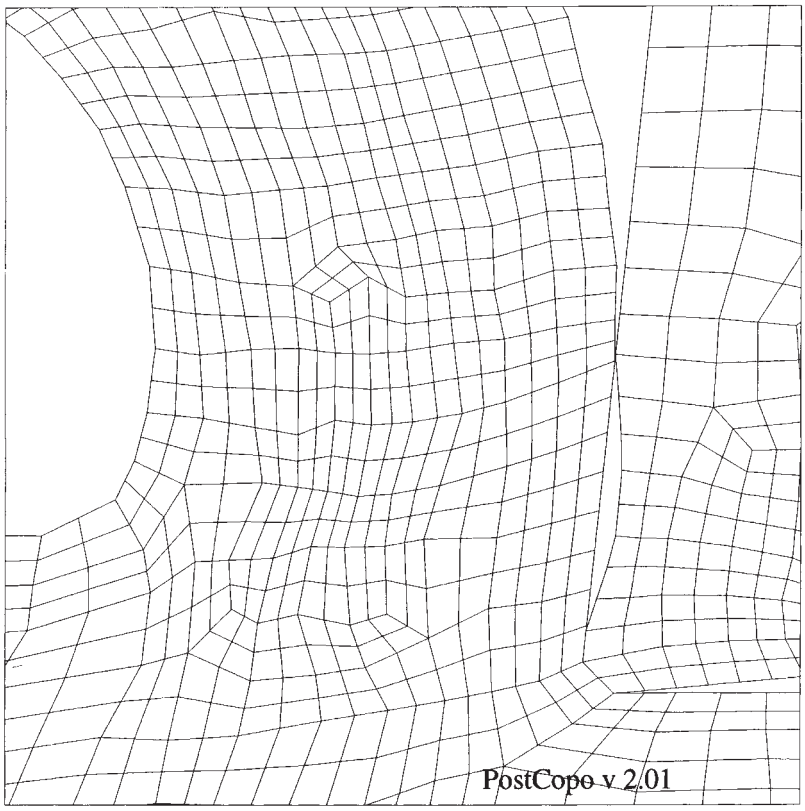

Fig. 9 Initial geometry for cutting with a cratered tool (depth of crater = 35 μm, length of crater = 0.45 mm)

respectively. The depths of cut were 0.25 and 0.5 mm, and three cutting speeds were chosen (1, 2 and 4 m/s).

In view of the comparison with the ALE model predictions, cutting tool forces were measured with a three-axis KISTLER dynamometer using piezoelectric sensors. The experimental chip thickness was also measured by means of a microphotograph and compared with the numerical values.

5 NUMERICAL RESULTS AND EXPERIMENTAL COMPARISONS

Under conditions identical to the metal-cutting experiments, the ALE method was used for the simulation of the process for comparison. The results illustrated in Figs 3 to 10 are relative to a simulation for which $V_c = 4$ m/s and $a_c = 0.25$ mm. A part of the initial control volume with the finite element and finite volume meshes of the workpiece and the tool are shown in Fig. 1. Figure 3 is associated with a non-stabilized and non-steady intermediate result: the velocity has a non-zero normal component on the free surfaces. The steady state velocity distribution and the corresponding geometry are given in Fig. 4. The distribution of the velocity vectors shows that the material is flowing upward at a fairly uniform speed. The velocity vectors change their direction and reduce speed in the so-called primary deformation zone [**2**]. Figure 5 shows the distribution of the von Mises stresses. The spatial variation of the von Mises stresses gives information on the orientation and the importance of the primary shear zone and those of the secondary shear zone. It is seen that the maximum value of about 1.030 GPa occurs in these regions. The location and magnitude of these high stresses have an important effect on the incipience of the material fracture and the subsequent discontinuous chip formation.

The contours of temperature during steady state cutting are shown in Fig. 6. The zone with the highest temperature occurs in the vicinity of the contact surface (secondary shear zone [**2**]). The maximum temperature is approximately 1000 °C and the highest temperature gradient is observed in the zone near the tool tip. The distribution in the tool shows that a high-temperature gradient is also observed in the vicinity of the tool tip and contact zone. These different phenomena were also observed in previous experimental works [**2**, **3**, **9**]. To verify the stability of the solution, the 'time history' can be plotted for different quantities. Figure 7 gives the evolution of node displacements on the free surface during the computing and Fig. 8 represents equivalent plastic strain evolutions in the vicinity of the contact surface (see Fig. 1 for the localization of corresponding nodes and elements). Note that these evolutions cannot be considered as a real transient solution because the initial geometry is arbitrary; these curves must be

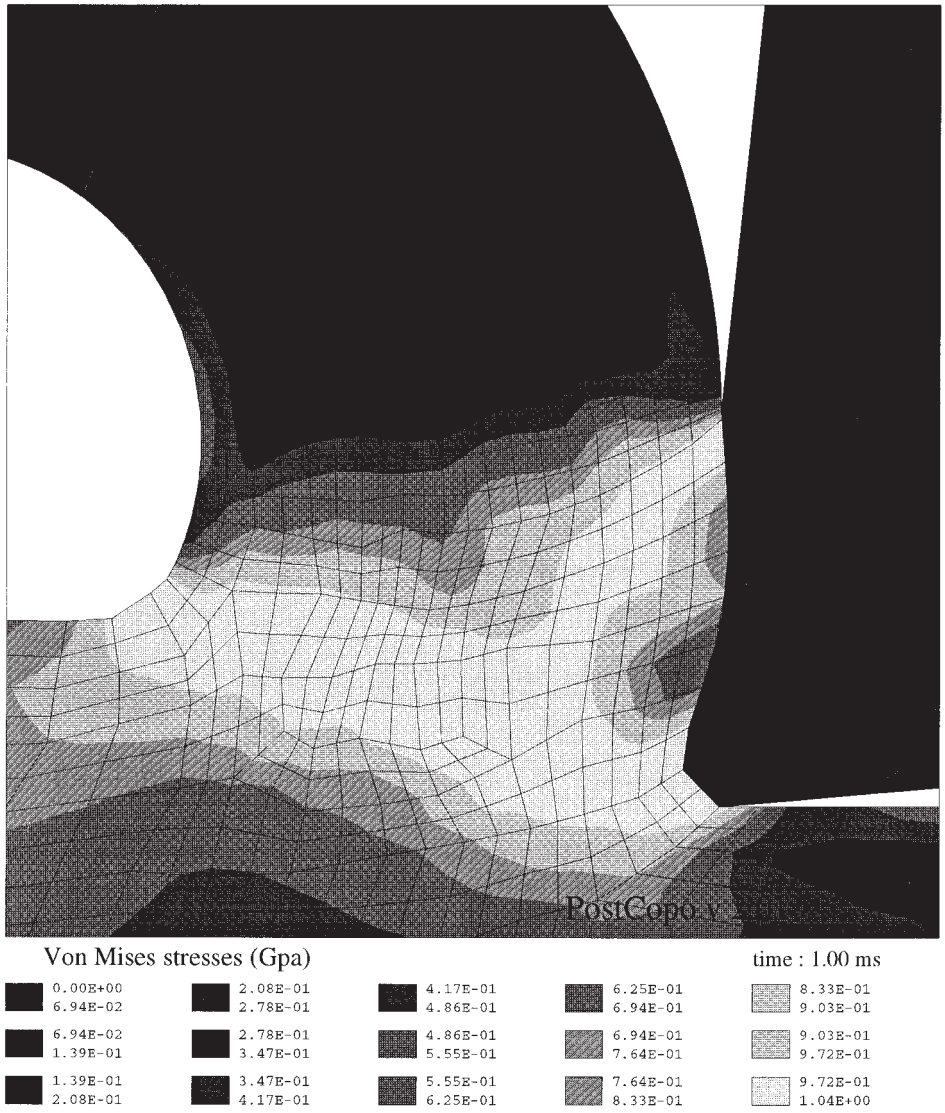

Fig. 10 Stabilized geometry and von Mises stresses for cutting with a cratered tool

interpreted as an evolution of variables during the free surface update procedure.

According to these different results, steady state conditions are practically achieved for chip geometry and all mechanical quantities. The stationarity of the temperature field in the chip and the workpiece is almost attained because the advection transfer is dominant in these domains. However, for the tool, the heat transfer is purely diffusive and temperatures are not stabilized because of the short duration of the cutting simulation. Concerning the convergence, the accuracy of the finite element technique depends on the size of the mesh; a model with a more refined mesh in the contact and tip tool zones does not change the results appreciably (3 per cent of variation for the maximum temperature between a '600 element' model and a '640 element' model). Finally, tool forces were computed by summing the forces acting on the tool rake face and decomposing them into the cutting and feed force components. The comparisons between the ALE model predictions and the experimental measurements are given in Table 1. In this table, the maximum value is given of the experimental chip thickness [CT (exp)] when the chip is scalloped.

It can be seen that correlation with a reasonable level of agreement was found between the measured chip thicknesses and those predicted by the ALE model over the entire range of depths of cut and cutting speeds tested. A similar agreement can also be observed for the cutting forces and the feed forces. The authors consider that the discrepancies can be attributed to the validity of the friction modelling and to the precision of material parameters. Both the experimental measurements and numerical predictions show a similar trend when compared with results obtained by other investigators using other materials (references [**2**], [**4**] and [**9**]).

Finally, Figs 9 and 10 are associated with a simulation of the cutting process with a cratered tool. These figures represent respectively the initial arbitrary geometry

(Fig. 9) and the stabilized geometry with the von Mises stresses field (Fig. 10). The influence of the crater on the numerical cutting force is significant: an increase of the order of 15 per cent was noted for simulated cases (for a crater of 0.35 μm of depth).

6 CONCLUSIONS

An arbitrary Lagrangian–Eulerian cutting model was used to simulate the orthogonal cutting process. The approach suggested here provides a solution to remedy the problems linked to the classical Lagrangian and Eulerian formulations, i.e. severe mesh distortion in the Lagrangian description and unknown boundaries and contact length in the Eulerian approach. Different results and observations obtained from the numerical model have been compared with experimental measurements of cutting force and chip thickness, and with other observations from the literature. The model constitutes a useful tool in predicting different variables during a cutting operation. Future works concern some investigations on material parameters (especially in viscoplasticity) and friction modelling. An extension may include shear band formation to simulate discontinuous chip formation and also three-dimensional modelling of the cutting process.

REFERENCES

1 **Strenkowski, J. S.** and **Carroll, J. T.** A finite element model of orthogonal metal cutting. *Trans. ASME, J. Engng for Industry*, 1985, **107**, 349–354.

2 **Oxley, P. L. B.** Modelling machining processes with a view of their optimization and to the adaptative control of metal cutting machine tools. *Robotics and Computer-Integrated Mfg*, 1988, **4**, 103–119.

3 **Childs, T. H. C.** and **Maekawa, K.** Computer-aided simulation and experimental studies of chip flow and tool wear, in the turning of flow alloy steels by cemented carbide tools. *Wear*, 1990, **139**, 235–250.

4 **Komvopoulos, K.** and **Erpenbeck, S. A.** Finite element modelling of orthogonal metal cutting. *Trans. ASME, J. Engng for Industry*, 1991, **107**, 253–265.

5 **Shih, A. J.** and **Yang, H. T. Y.** Experimental and finite element predictions of residual stresses due to orthogonal metal cutting. *Int. J. Numer. Meth. Engng*, 1993, **36**, 1487–1507.

6 **Shekon, G. S.** and **Chenot, J. I.** Numerical simulation of continuous chip formation during non-steady orthogonal metal cutting. *Engng Comput.*, 1993, **10**, 31–48.

7 **Marusich, T. D.** and **Ortiz, M.** Modelling and simulation of high-speed machining. *Int. J. Numer. Meth. Engng*, 1995, **38**, 3675–3694.

8 **Zienkiewicz, O. C., Jain, P. C.** and **Onate, O. C.** Flow of solids during forming and extrusion: some aspects of numerical solution. *Int. J. Solids Structs*, 1978, **14**, 15–38.

9 **Strenkowski, J. S.** and **Moon, K. J.** Finite element prediction of chip geometry and tool workpiece temperature in orthogonal metal cutting. *Trans. ASME, J. Engng for Industry*, 1990, **112**, 313–318.

10 **Donnea, J., Giuliani, S.** and **Halleux, J. P.** An arbitrary Lagrangian Eulerian finite element method for transient dynamic fluid structure interaction. *Comput. Meth. Appl. Mech. Engng*, 1982, **33**, 689–723.

11 **Huentink, J., Vreede, P. T.** and **Van Der Lugt, J.** Progress in mixed Eulerian Lagrangian finite element simulation of forming process. *Int. J. Numer. Meth. Engng*, 1990, **30**, 1441–1457.

12 **Liu, W. K., Belytschko, T.** and **Chang, H.** An arbitrary Lagrangian–Eulerian method for path-dependent materials. *Comput. Meth. Appl. Mech. Engng*, 1986, **58**, 227–245.

13 **Rakotomalala, R., Joyot, P.** and **Touratier, M.** An arbitrary Lagrangian–Eulerian thermomechanical finite element model of material cutting. *Comput. Numer. Meth. Engng*, 1993, **9**, 975–987.

14 **Johnson, G. R.** and **Cook, W. H.** A constitutive model and data for metal subjected to large strains, high strain rates and high temperatures. In Proceedings of 7th International Symposium on *Balistics*, The Hague, 1983, pp. 12–21.

15 **Kosloff, D.** and **Frazier, G.** Treatment of hourglass pattern in low order finite element code. *Int. J. Numer. Meth. Geomechanics*, 1978, **2**, 57–72.

16 **Patankar, S. V.** *Numerical Heat Transfer and Fluid Flow*, 1980, Series in Computational Methods in Mechanics and Thermal Sciences (Hemisphere Publishing Corporation, New York).

17 **Giuliani, S.** An algorithm for continuous rezoning of the hydrodynamic grid in arbitrary Lagrangian Eulerian computer codes. *Nucl. Engng Des.*, 1982, 205–212.

18 **Bois, D.** and **Grave, A.** Simulation numérique d'essais d'impact et comparaison de lois de comportement. *J. de Physique*, 1985, **46**, 101–112.